Binocular adaptive optics vision analyzer with full control over the complex pupil functions

Christina Schwarz, Pedro M. Prieto, Enrique J. Fernández, and Pablo Artal*

Laboratorio de Óptica, Instituto Universitario de investigación en Óptica y Nanofísica, Universidad de Murcia, Campus Espinardo (Edificio 34), E-30100 Murcia, Spain

**Corresponding author: pablo@um.es*

Received August 17, 2011; revised October 3, 2011; accepted October 3, 2011; posted October 7, 2011 (Doc. ID 152992); published December 14, 2011

We present a binocular adaptive optics vision analyzer fully capable of controlling both amplitude and phase of the two complex pupil functions in each eye of the subject. A special feature of the instrument is its comparatively simple setup. A single reflective liquid crystal on silicon spatial light modulator working in pure phase modulation generates the phase profiles for both pupils simultaneously. In addition, another liquid crystal spatial light modulator working in transmission operates in pure intensity modulation to produce a large variety of pupil masks for each eye. Subjects perform visual tasks through any predefined variations of the complex pupil function for both eyes. As an example of the system efficiency, we recorded images of the stimuli through the system as they were projected at the subject's retina. This instrument proves to be extremely versatile for designing and testing novel ophthalmic elements and simulating visual outcomes, as well as for further research of binocular vision.

OCIS codes: 010.1080, 330.4460.

Since their first introduction about 10 years ago [1], adaptive optics (AO) visual simulators, or vision analyzers, have become an important new tool for studying spatial vision [2–4] and designing and testing new ophthalmic correction devices and procedures [5–7]. These instruments are based on a visual testing unit projecting stimuli, combined with a wavefront sensor to measure the subject's ocular aberrations and a wavefront corrector to induce a desired aberration pattern. While the first generation was designed as monocular devices [8], more recent versions also permit AO visual testing under binocular conditions [9,10]. These recent instruments used liquid crystal spatial light modulators (LC-SLMs) for wavefront modulation. These devices offer several advantages compared to deformable mirrors, regarding user friendliness, resolution, and in some cases, cost. However, drawbacks of LC devices still persist [11], especially concerning response speed, diffraction effects, wavelength dependent behaviors, and requirement of polarized light, although the latter is of no relevance for visual testing [12].

In the following, we present a new and improved version of a binocular AO vision analyzer featuring full computer-based control over the two complex pupil functions. The instrument allows for visual testing under actual binocular vision while optical aberrations and pupil apertures of both eyes simultaneously can be manipulated by means of LC-SLMs. A schematic diagram of the entire setup is shown in Fig. 1. The system is based on previous versions developed in our laboratory [9,10]. A collimated beam from a laser emitting light at 780 nm is divided into two separate narrow beams by means of a mask with two circular apertures of 1 mm diameter. Each beam enters the corresponding eye of the subject via a pellicle beam splitter (PBS) and a binocular periscope system consisting of two mirrors on kinematic mirror mounts M1 and M2 and prism mirror P. Since alignment of the subject's pupils and line of sight is a critical point, the binocular periscope system allows for horizontal, vertical, and angular fine adjustment of the light beams. A dental impression mount attached to a translation stage is used to stabilize the subject's head and provides accurate pupil positioning. The reflected and backscattered light from the eye re-enters the optical system via the periscopic system and both pupils are projected onto a Hartmann–Shack lenslet array with 200 μm microlens pitch and a focal length of 6 mm. A telescope system, composed of two achromatic doublets, L1 and L6, conjugates the sensor to the subject's pupil plane, introducing a magnification factor of 0.5. That way, a natural pupil of 4 mm diameter is sampled by more than 75 microlenses. Hence, it is possible to measure the ocular aberrations of both eyes simultaneously by means of a single Hartmann–Shack sensor (HSS). The procedure to estimate the two eyes' aberrations from the Hartmann–Shack spot images is described elsewhere [13]. Pupil positions and lines of sight were checked by using an additional pupil camera (not shown in Fig. 1 for clarity).

Once the alignment procedure and aberration measurement are performed, the flip mirror (FM) is moved

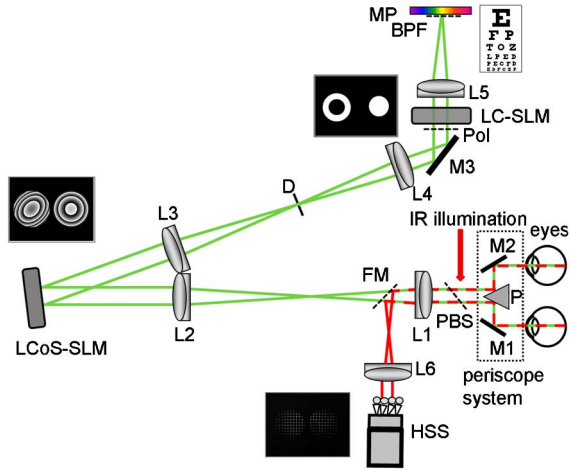

Fig. 1. (Color online) Schematic view of the LC-based instrument. See text for detailed description.

out from the beam and the subject is able to see the presented stimulus through the system. The system in the current mode of operation performs only static correction/manipulation of aberrations. As a stimuli generator, we use a modified microprojector (MP), (3M Projection Systems, 3M Pocket Projector MPro120). The projector objective was removed and replaced by an achromatic doublet of a focal length of 200 mm (L5). In addition, diffusers were placed in front of the back-illuminating three-color (red–green–blue) LED array. The actual microdisplay consists of a matrix of 640×480 square pixels measuring 11.75 μm in size. Because of an antialiasing technique automatically performed by the projector hardware, an effective resolution of 800×600 pixels (pixel size 9.4 μm) is created. The projector delivers 12 lm and the emitted light is horizontally polarized. A bandpass filter (BPF) with a central wavelength of 550 nm and 40 nm bandwidth is placed in front of the microprojector. A gamma factor of about 2.7 was measured, which is taken into account by the visual testing control software package. This was developed in MATLAB (Mathworks) and allows presenting different types of stimuli, e.g., tumbling E or gratings, based on the psychophysics toolbox extensions [14].

To create the entrance pupils, we incorporated an optically addressed LC-SLM of a transmissive type (Holoeye Photonics AG, LC2002). The active area measures $26.6\,\text{mm} \times 20\,\text{mm}$ and is controlled by 800×600 pixels. The manufacturer specifies a maximum refresh frame rate of 60 Hz. The input director orientation Ψ_D was found to be at 45° approximately. Placed in between crossed (or parallel) polarizers, the device operates in pure intensity modulation. Since the light emitted by the stimuli microprojector is already horizontally polarized, we rotated the LC-SLM by 45°, so that the input director axis coincides with the axis of polarization. Because of this configuration, merely an analyzer (Pol) is required. The calibration procedure consisted of determination of the transmitted intensity for displayed flat images of distinct 8 bit gray values, once the analyzer angle was correctly set. The calibration curve showed that an intensity difference of 80% is achieved by a gray-level difference of about 60, so that the device permits rough transmittance control. Additionally, we measured possible induced phase changes by means of the HSS when the modulator was in pure intensity configuration and intensity gradient pupils of different diameters were set. The root mean squared changes in the induced wavefronts were of the order of nanometers for pupils up to 8 mm in diameter and, therefore, negligible. The control software was written in MATLAB and enabled pupil positioning, transmittance control and setting aperture diameters of differently shaped pupils after including the calibration curve mentioned above.

The LC-SLM is conjugated with the eyes' pupil plane, so that any desired pupil mask as to size, location, shape, and transmittance can be created. Examples of different pupil shapes and intensity profiles are presented in Fig. 2. Generating artificial pupils by a transmissive intensity modulator has several advantages over the milled pupil masks typically used in optical setups. First of all, the alignment procedure is facilitated to a great extent. The modulator roughly has to be placed in the required position and fine adjustment can be performed by moving the generated pupils on the LC array via the software. Second, the milled pupil masks have to be replaced and realigned every time the pupil diameter is changed, either by hand or via motorized stages. Finally, the LC-SLM in pure intensity configuration permits generating pupils that are extremely challenging to create by manufactured masks, such as the ring-shaped pupil or the gradient pupil presented in Figs. 2(a) or (b), respectively. However, a drawback of the device is the observed diffraction effect since the pixel array of the LC acts as an optical grid. First-order diffraction images appear at a visual angle of 0.96°, which is why we had to restrict the visual testing field to a circular region of about 0.9° in diameter and additionally block higher-order images by means of a diaphragm (D) in the conjugate image plane next to the intensity modulator.

Aberration correction and manipulation is performed by a reflective LCoS-SLM (Hamamatsu Photonics, LCoS-SLM X10468-04). The plane of the LC-SLM is optically conjugated to the plane of the phase modulator via a relay telescope composed of two achromatic doublets, L3 and L4, providing a magnification factor of 1.25. The LCoS-SLM is an optically addressed device with an array of 800×600 independent silicon pixels (corresponding to a region of $16\,\text{mm} \times 12\,\text{mm}$) in direct contact with the parallel-aligned nematic LC. The voltage of each pixel is controlled by a gray-level image, also 800×600 pixels in size. Phase modulation is achieved by locally changing the refractive index of the LC due to voltage modification of the corresponding neighboring silicon pixel. Accurately calibrated, the wavefront modulator shows a precise performance [15], which makes it appropriate for open-loop high-resolution wavefront control. In case of natural pupils of 4 mm in diameter, each pupil is sampled by about 49000 independent pixels to modulate the wavefront. Control software was written in MATLAB and has been explicitly described elsewhere [8]. This device is also affected by diffraction effects, but the first-order images appear at larger angles from the zero-order image, so that visual testing is not affected when properly masked. Another relay telescope, composed of two achromatic doublets, L1 and L2, conjugates the wavefront modulator plane with the subject's pupil plane. There is unity magnification between the artificial pupil plane and the natural pupil plane.

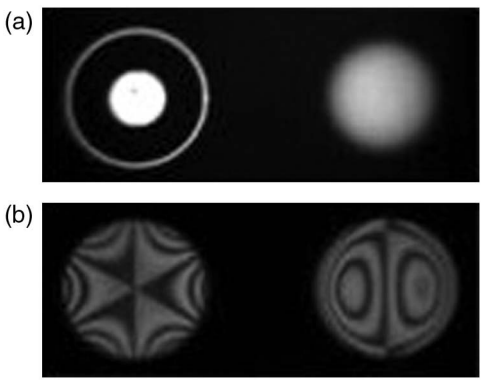

Fig. 2. Images of pupil planes when setting pupil apertures with the LC-SLM [(a) and (b)].

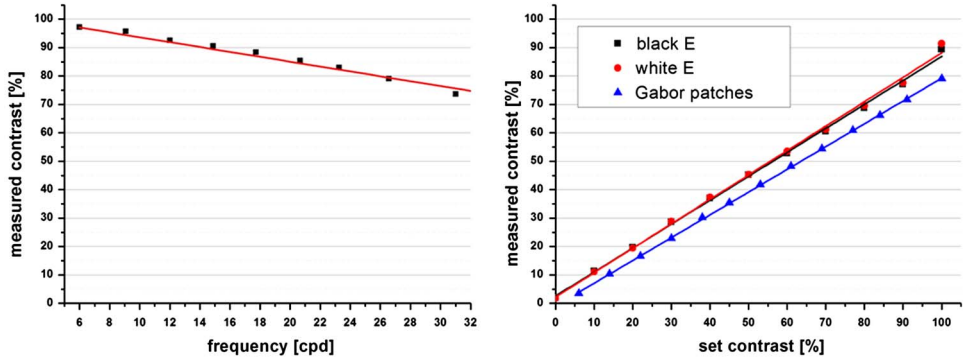

Fig. 3. (Color online) Measured contrast versus frequency and versus set contrast, respectively.

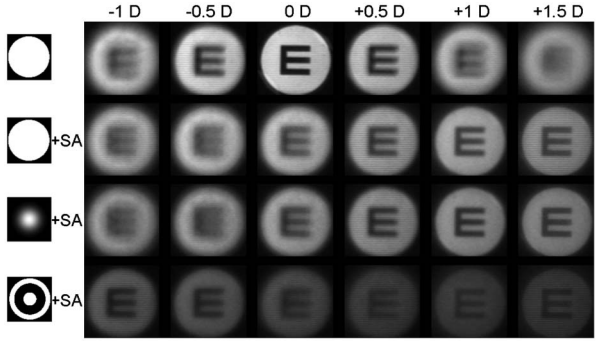

Fig. 4. Images of a letter E, subtending 0.4 deg, taken through the AO instrument for different pupil shapes (marked on the left) with or without induced spherical aberration (SA).

The contrast of projected stimuli is likely to be affected by the diffractive elements and by the antialiasing technique of the microprojector itself. This could have important practical implications. We measured the actual contrast by placing an external additional CCD camera at one of the subject's eyes' positions and took images of letters or gratings of different frequencies presented by the stimulus generator. For increasing frequencies, contrast decreases linearly when maintaining theoretical contrast at 100% (Fig. 3). The tested frequency range was chosen according to the range typically used for visual testing. In addition, we measured the effective system contrast when reducing theoretical contrast for different types of stimuli of a frequency of 6 cpd. In case theoretical contrast was reduced, measured contrast was also found to be linearly reduced. These contrast behaviors were corrected for in the visual testing software.

Finally, to better shows the system performance, we placed a CCD camera with a 28 mm objective of a relative aperture of $f/3.5$ at one of the exit pupils of the simulator and took images of the presented stimuli through the system for different combinations of pupil shapes and aberration patterns (Fig. 4). The first line represents through focus images of a letter E recorded for a circular pupil in absence of any higher-order aberrations, whereas the lines underneath show stimuli when spherical aberration is present and the pupil is circular, a Gaussian intensity profile, or a binary ring shape, respectively. Although the actual shape of the pupil has a minor impact on the formed images, a change in contrast and blur can be observed.

In summary, we developed a novel LC-based binocular AO vision analyzer that is not only capable of manipulating aberrations for both eyes, but is also efficient for controlling pupil shape and transmittance. This instrument allows modification of the two complex pupil functions in the eyes. This means a full control on all the possible optical properties of the eyes. Therefore, the technique is appropriate for investigating different aspects of how optics affects binocular vision and the development of improved ophthalmic elements of refractive surgery procedures. As an example, the instrument could be used for testing the potential and limitations of corneal or lenticular implants inducing intensity transmission gradients, which can be easily simulated with the system in combination with any desired induced aberration.

This work was supported by the "Ministerio de Ciencia e Innovación," Spain (grants FIS2010-14926 and CSD2007-00013) and Fundación Séneca (Region de Murcia, Spain), grant 4524/GERM/06.

References

1. E. J. Fernández, S. Manzanera, P. Piers, and P. Artal, J. Refract. Surg. **18**, S634 (2002).
2. P. Artal, L. Chen, E. J. Fernández, B. Singer, S. Manzanera, and D. R. Williams, J. Vis. **4**, 281 (2004).
3. G. Pérez, S. Manzanera, and P. Artal, J. Vis. **9**, 19 (2009).
4. E. A. Rossi, P. Weiser, J. Tarrant, and A. Roorda, J. Vis. **7**, 14 (2007).
5. P. A. Piers, E. J. Fernández, S. Manzanera, S. Norrby, and P. Artal, Invest. Ophthalmol. Vis. Sci. **45**, 4601 (2004).
6. S. Manzanera, P. M. Prieto, D. B. Ayala, J. M. Lindacher, and P. Artal, Opt. Express **15**, 16177 (2007).
7. J. Tabernero, C. Schwarz, E. J. Fernandez, and P. Artal, Invest. Ophthalmol. Vis. Sci. **52**, 5273 (2011).
8. E. J. Fernández, I. Iglesias, and P. Artal, Opt. Lett. **26**, 746 (2001).
9. E. J. Fernández, P. M. Prieto, and P. Artal, Opt. Lett. **34**, 2628 (2009).
10. E. J. Fernández, P. M. Prieto, and P. Artal, **27**, A48 (2010).
11. P. M. Prieto, E. J. Fernandez, S. Manzanera, and P. Artal, Opt. Express **12**, 4059 (2004).
12. P. M. Prieto, F. Vargas-Martin, J. S. Mc Lellan, and S. A. Burns, J. Opt. Soc. Am. A **19**, 809 (2002).
13. P. M. Prieto, F. Vargas-Martin, S. Goelz, and P. Artal, J. Opt. Soc. Am. A **17**, 1388 (2000).
14. D. G. Pelli, Spatial Vis. **10**, 437 (1997).
15. E. J. Fernández, P. M. Prieto, and P. Artal, Opt. Express **17**, 11013 (2009).